Computational Materials Science 188 (2021) 110128

Contents lists available at ScienceDirect

Computational Materials Science

journal homepage: www.elsevier.com/locate/commatsci

Pseudoelasticity in twinned α-Fe nanowires under bending

Yang Yang, Suzhi Li *, Xiangdong Ding *, Jun Sun

State Key Laboratory for Mechanical Behavior of Materials, Xi'an Jiaotong University, Xi'an 710049, China

ARTICLE INFO

Keywords:
Bending
Twinned nanowires
Pseudoelasticity
Dislocations
Size effect

ABSTRACT

The pre-existing twin boundaries play an important role in the mechanical behaviors of metals. In the present work, we studied the bending deformation of [100]-oriented α-Fe nanowires seeded with ⟨111⟩/{112} twin boundaries using atomistic simulations. Bending behaviors along two different orientations were investigated. The initially flat twin boundaries become curved with a high density of 1/6 ⟨111⟩/{112} partial dislocations under bending when the neutral plane intersects with twin plane along [0$\bar{1}$1] direction, whereas could transform to the nonconventional {110} interfaces under bending when the neutral plane intersects with twin plane along [111] direction. The bent α-Fe nanowires could recover to the original state upon unloading, leading to a unique pseudoelasticity. The driving force for shape recovery primarily arises from the high interfacial energy, i.e. curved {112} twin boundaries or the transformed {110} interfaces. We further characterized the recoverability by the ratio η of the nanowire size (external length scale) to twin boundary spacing (internal length scale). This η-dependent recoverability matches well with the experimental data at large length scale. The present work may help understand the unique mechanical properties associated with twin boundaries in metals.

1. Introduction

With the decrease of the sample size, the yielding stress greatly increases, making the twinning a preferred deformation mode at small scale [1–3]. The deformation twinning is observed to be reversible experimentally in body-centered cubic (bcc) tungsten nanocrystals. This makes the materials to exhibit a unique pseudoelastic behavior [1–3], which keeps accordance with the early results by molecular dynamics simulations [4–6]. The good recoverability origins from the reversible twinning with the aid of 1/6 ⟨111⟩ partial dislocations. The driving force can be stored at surfaces [4], grain boundaries [1] or twin boundaries (TBs) [6]. For example, some bcc metal nanowires exhibit pesudoelasticity by a "reversible" twinning mechanism [4,5]. The driving force arises from the large difference of surface energies between the twinned and un-twinned states [4]. Bending a [100]-oriented α-Fe nanowires could induce the formation of the nonconventional {110} interfaces [6]. The gradient stress induces ⟨111⟩/{112} twins in each atomic layer with different thickness. A series of adjacent {112} twin boundaries pile up to form this {110} interface [6]. The {110} interface has a high interfacial energy and provides the primary driving force for shape recovery. The pseudoelasticity of bcc metals shows great potential applications in functional devices such as nano-springs, actuators and sensors.

When the sample is seeded with TBs, the recoverability could be largely enhanced [7,8]. For example, the six-fold twinned α-Fe nanowire can be totally "untwisted" by the reverse motion of twin boundaries, leading to huge pseudoelasticity. The penta-twinned silver nanowires show the reversible plasticity due to the reverse motion of partial dislocations driven by the repulsive force from the twin boundaries [9]. Bending induced pseudoelasticity in twinned materials has been experimentally observed in bulk materials such as Cu-Al-Ni [10] and In-Tl alloys [11]. However, the microscopic origin for such pseudoelasticity in twinned structures remains unclear.

Here we studied the bending deformation in twinned α-Fe nanowires using molecular dynamics simulations. The shape recovery of bending are related to the pre-existing TBs. Depending on the bending orientations, the pre-existing TBs could either become with a high density of partial dislocations or transform to a nonconventional {110} interface. The bent samples show good recoverability upon unloading. We probe the microscopic mechanisms of such novel pseudoelasticity. We found the maximum recoverable strain could be characterized by a ratio η of the external length (wire side width) to the internal length (twin boundary spacing). Our work might provide the insight on bending-induced pseudoelasticity in bulk Cu-Al-Ni [10] and In-Tl alloys [11,12] experimentally, and also help to design smart devices based on domain boundary engineering [13].

* Corresponding authors.
E-mail addresses: lisuzhi@xjtu.edu.cn (S. Li), dingxd@mail.xjtu.edu.cn (X. Ding).

https://doi.org/10.1016/j.commatsci.2020.110128
Received 22 July 2020; Received in revised form 24 September 2020; Accepted 8 October 2020
Available online 16 November 2020

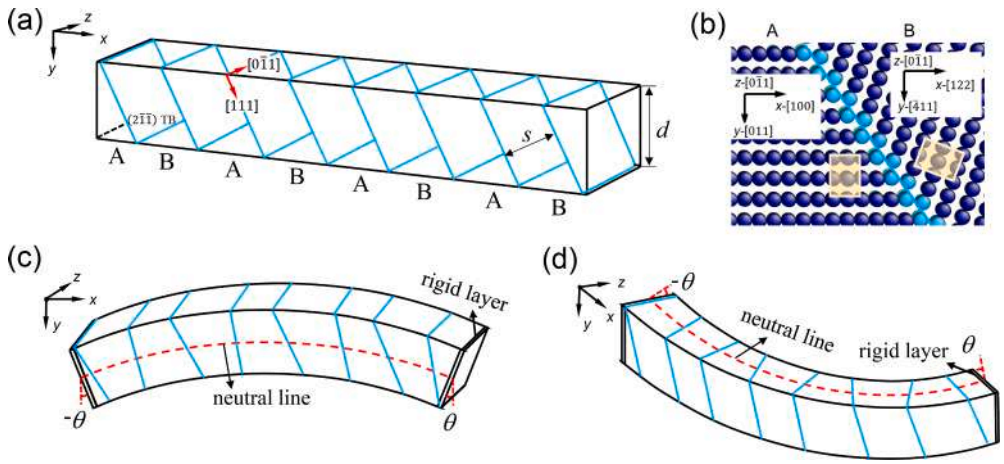

Fig. 1. (a) Schematic illustration of the α-Fe nanowire seeded with ⟨111⟩/{112} twin boundaries. (b) The sample contains two variants. (c) *xy*-bending and (d) *xz*-bending by tilting the rigid layers at both ends of the nanowire.

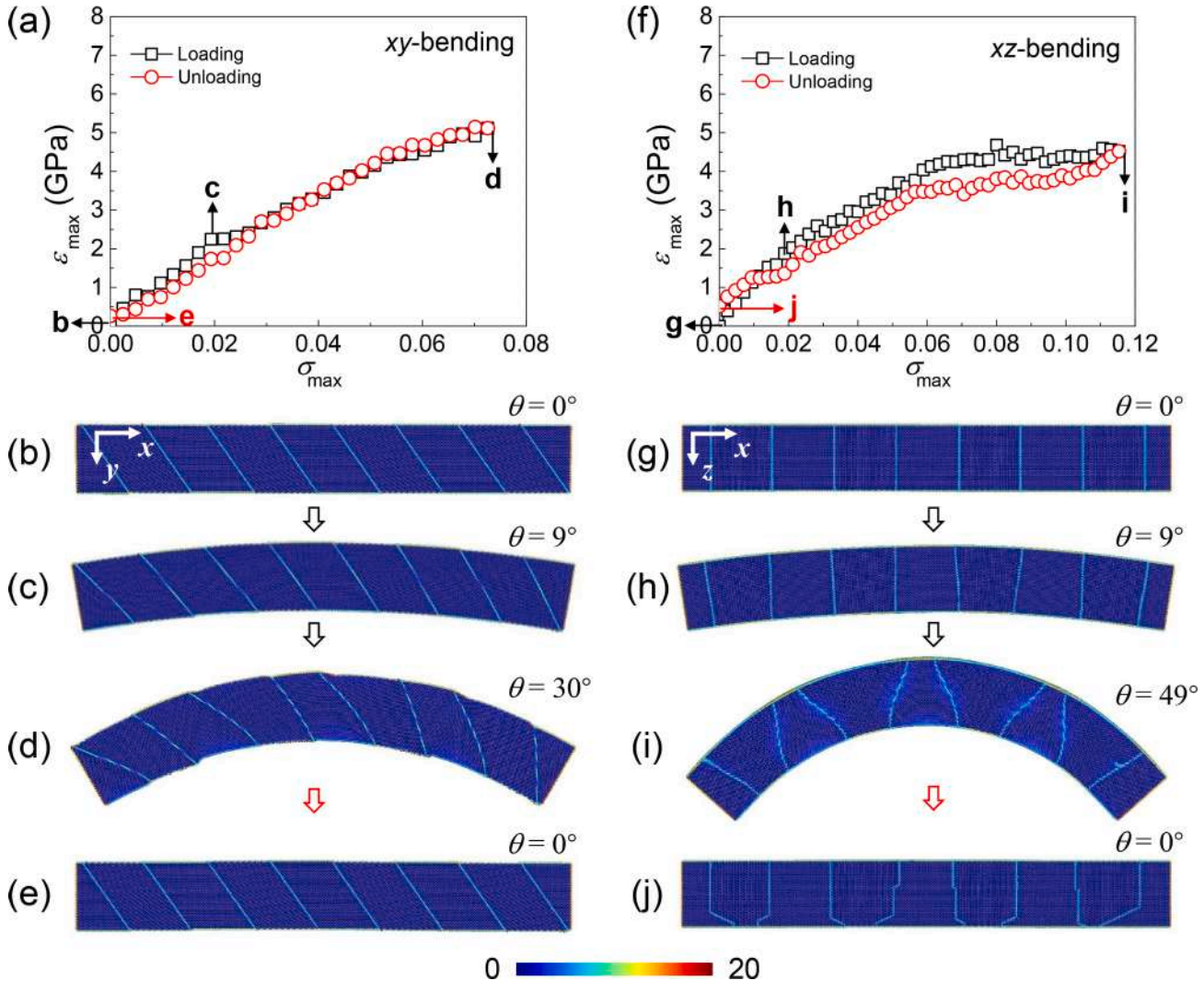

Fig. 2. Bending deformation of a twinned α-Fe nanowire at 300 K (d = 10.0 nm, s = 8.0 nm). (a) Maximum tensile stress σ_{max} *vs* maximum tensile strain ε_{max} curves for the *xy*-bending. (b)-(e) Typical atomic images upon loading and unloading for the *xy*-bending. (f) Maximum tensile stress σ_{max} *vs* maximum tensile strain ε_{max} curves for the *xz*-bending. (g)-(j) Typical atomic images upon loading and unloading for the *xz*-bending. The colors are coded according to the centrosymmetry parameters [25].

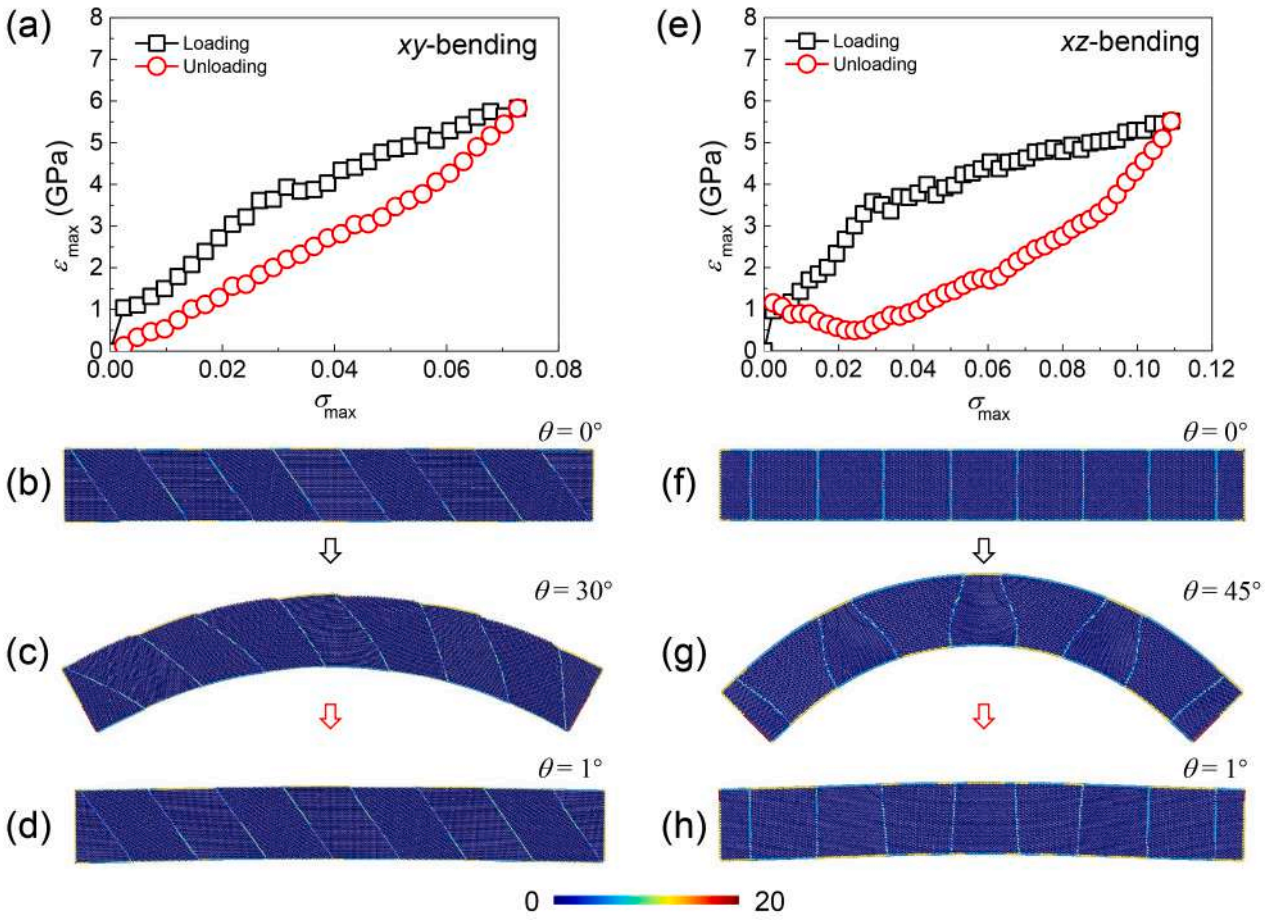

Fig. 3. Bending deformation of a twinned α-Fe nanowire via molecular statics simulations (d = 10.0 nm, s = 8.0 nm). (a) Maximum tensile stress σ_{max} *vs* maximum tensile strain ε_{max} curves for the *xy*-bending. (b)-(d) Typical atomic images upon loading and unloading for the *xy*-bending. (e) Maximum tensile stress σ_{max} *vs* maximum tensile strain ε_{max} curves for the *xz*-bending. (f)-(h) Typical atomic images upon loading and unloading for the *xz*-bending. The colors are coded according to the centrosymmetry parameters [25].

2. Methods

We used the embedded atom method (EAM) developed by Mendelev et al. to describe the interatomic interactions in α-Fe [14,15]. This empirical potential can reproduce various properties and has been used to study the mechanical behaviors of α-Fe in many atomistic simulations. Fig. 1a shows the model of the [100]-oriented α-Fe nanowires seeded with $(2\bar{1}\bar{1})$ twin boundaries. It contains two variants A and B with the orientations of *x*-[100], *y*-[011], *z*-$[0\bar{1}1]$ and *x*-[122], *y*-$[\bar{4}11]$, *z*-$[0\bar{1}1]$ (Fig. 1b), respectively. The aspect ratio is fixed to be around 7. Two length-scales are characterized as wire side width d (external length) and twin boundary spacing s (internal length). We performed a set of simulations with d varying from 5.0 nm to 15.0 nm, and s varying from 1.0 nm to 60.0 nm. All the molecular dynamics simulations were carried out at 300 K, which is above the brittle-ductile transition temperature of 130 K ~ 150 K in α-Fe [16]. Before bending, the nanowires were relaxed at 300 K using a Nosé-Hoover thermostat [17,18]. Several atomic layers at both ends of the nanowire were fixed rigidly as the loading grips. Bending is induced by tilting the rigid loading ends against each other. The tilt was increased stepwise by $\Delta\theta = 1^\circ$ and relaxed at 300 K for 0.1 ns, where θ is the bending angle defined as half of the inclination angle of the two fixed surface layers against each other. We compared the mechanical behaviors with bending moment applied in two separate orientations, i.e. *xy*-bending with the neutral plane intersects with twin plane along $[0\bar{1}1]$ direction (Fig. 1c) and *xz*-bending with the neutral plane intersects with twin plane along [111] direction (Fig. 1d). Unloading was performed in a similar way by reducing the bending angle. We use the maximum tensile stress σ_{max} and the maximum tensile strain ε_{max} to characterize the bending behavior in different samples. The maximum tensile strain ε_{max} is calculated as the bending angle θ divided by the aspect ratio of the sample, $\varepsilon_{max} = \theta d/L$. The maximum tensile stress is $\sigma_{max} = -Md/(2I)$, where M is the bending moment, I is the moment of inertia and $d/2$ is the distance from the neutral line to the surface of the nanowires. The calculations were carried out using LAMMPS code [19] and the atomic configurations were displayed by AtomEye [20]. The type and configurations of dislocations generated during deformation was detected using Ovito [21,22].

3. Results

3.1. Pseudoelasticity in twinned α-Fe nanowires under bending

Fig. 2 shows the pseudoelasticity in a twinned nanowire (d = 10.0 nm, s = 8.0 nm) under both *xy*- and *xz*-bending. The variation of σ_{max} as a function of ε_{max} in *xy*-bending is shown in Fig. 2a. The twinned nanowire first undergoes an elastic deformation and then yields with σ_{max} = 2.2 GPa at ε_{max} = ~2%. The nanowire shows a strong strain hardening after yielding. The stress can almost retrace back upon unloading at ε_{max} = ~7%, leading to a typical pseudoelasticity. For comparison, the maximum recoverable strain is ca. 0.05% for bulk iron [23] and ca. 1.4% for iron whiskers [24]. The motion of twin boundaries upon loading and unloading is reversible, as the typical images shown in

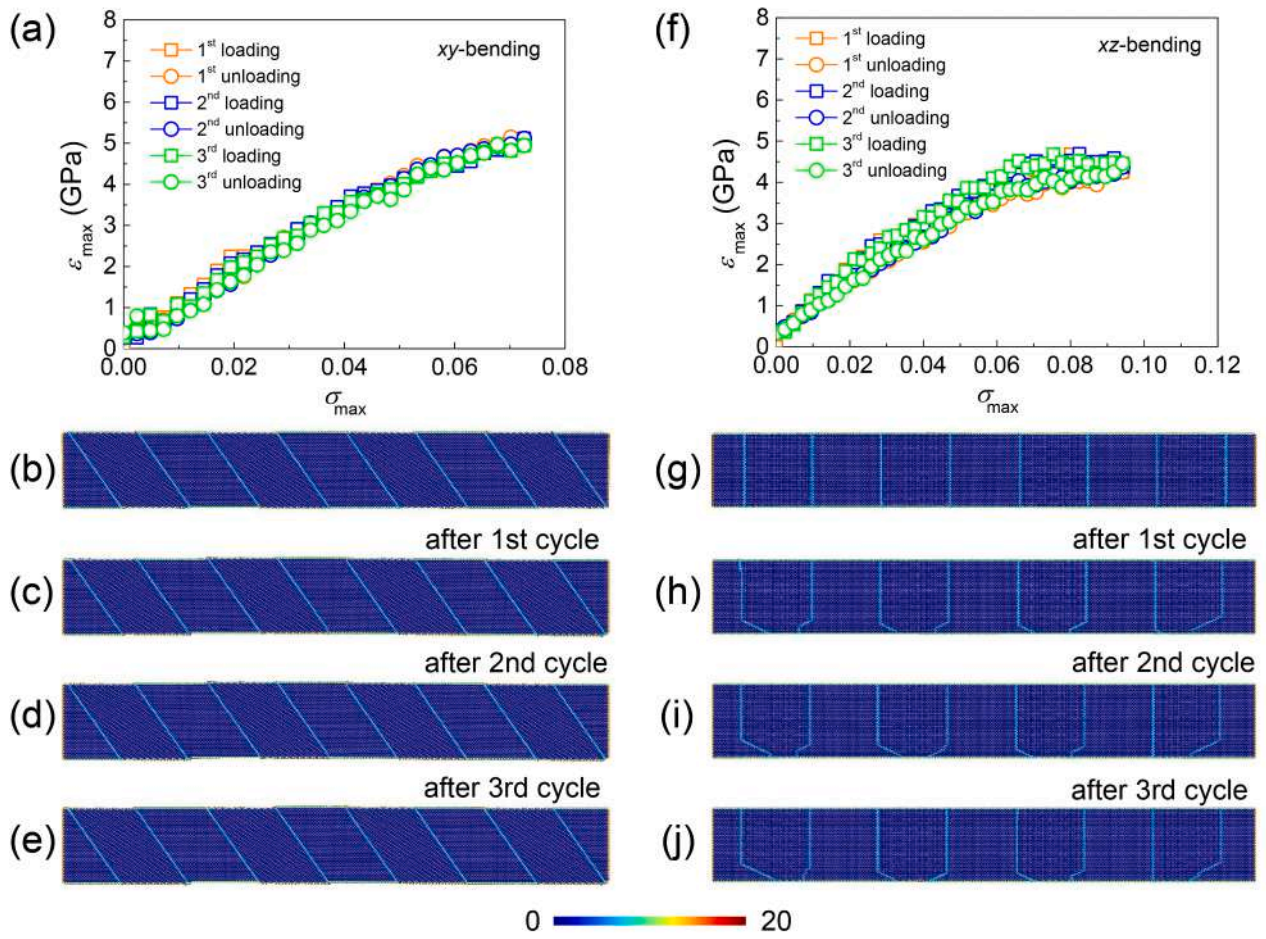

Fig. 4. Cyclic loading for bending-induced pseudoelasticity in a twinned α -Fe nanowire at 300 K ($d = 10.0$ nm, $s = 8.0$ nm). (a) The variation of σ_{max} with ε_{max} at the first three loading–unloading cycles for the *xy*-bending. (b) The initial configuration of the undeformed nanowire. (c)-(e) The full recovered configurations after cyclic loading for the *xy*-bending. (f) The variation of σ_{max} with ε_{max} at the first three loading–unloading cycles for the *xz*-bending. (g) The initial configuration of the undeformed nanowire. (h)-(j) The recovered configurations after cyclic loading for the *xz*-bending. The colors are coded according to the centrosymmetry parameters [25].

Fig. 2b-e. The boundary motion is completed via the glide of partial dislocations. The non-deformed twin boundary lies perfectly at the $(2\bar{1}1)$ twin planes at $\theta = 0°$ (Fig. 2b). Partial dislocations start to nucleate from the surfaces in the tensile region and form steps at the twin boundaries on the incipient plasticity. More partials are stored in the bent sample with several steps at $\theta = 30°$ (Fig. 2d). In addition, we observed the {100} facets forms in the original {110} free surfaces under bending. After releasing the bending moment, the bent TBs become straight again, leading to a full recovery (Fig. 2e).

Fig. 2f shows the variation of σ_{max} as a function of ε_{max} for the *xz*-bending. The nanowire yields at $\varepsilon_{max} = \sim 2\%$ with a lower yield stress of $\sigma_{max} = 2.0$ GPa. The nanowire shows a similar strain hardening after yielding until $\varepsilon_{max} = \sim 6\%$. After that, the σ_{max} remains ~4.0 GPa. In comparison with the *xy*-bending, the nanowire shows a better recoverability with the maximum recoverable strain exceeding 10%. Fig. 2g-j show the typical atomic images upon loading and unloading in the *xz*-bending. The original paralleled straight TBs become curved and the domains become wedged under bending (Fig. 2i). Some {100} facets forms at the {110} free surfaces. Upon unloading, the twin patterns do not fully recover back.

The bending-induced pseudoelasticity is close related to movement of twin boundaries in twinned α-Fe nanowire. To exclude possible effects induced by high strain rates of molecular dynamics simulations, we performed another set of simulations to bend the nanowires using the molecular statics technique. The energy is minimized based on the conjugate gradient algorithm. Similar results were obtained, as shown in Fig. 3.

We further tested the shape recovery under cyclic loading. Fig. 4a shows the variation of σ_{max} as a function of ε_{max} for cyclic *xy*-bending. After each loading–unloading, the nanowire recovers back to its original state (Fig. 4b-e), leading to the pseudoelasticity. For the *xz*-bending, although some defects are left after the first cyclic loading, the shape recoverability is not affected significantly (Fig. 4f-j).

3.2. Mechanisms of shape recovery for pseudoelasticity

For the *xy*-bending, the reversible motion of twin boundaries is responsible for the shape recovery, as the typical images shown in Fig. 5a-d. The boundary motion is completed via the glide of partial dislocations. Originally the non-deformed twin boundary lies perfectly in the $(2\bar{1}1)$ plane at $\theta = 0°$ (Fig. 5a). The 1/6 ⟨111⟩/{112} partial dislocations start to nucleate and form steps at the twin boundaries at the yield point (Fig. 5b). The partials were identified to be the edge type. We observed more partials are generated and stored at the twin planes with large deformation ($\varepsilon_{max} \sim 7\%$, Fig. 5c). The density of partial dislocations could reach a high value ~0.4 nm^{-1} per TB. After releasing the bending moment, the bent TBs recover to the flat state again by the reverse motion of partial dislocations (Fig. 5d).

For the *xz*-bending, we observed that the shape recovery is achieved by the transformation of pre-existing twin boundaries to the

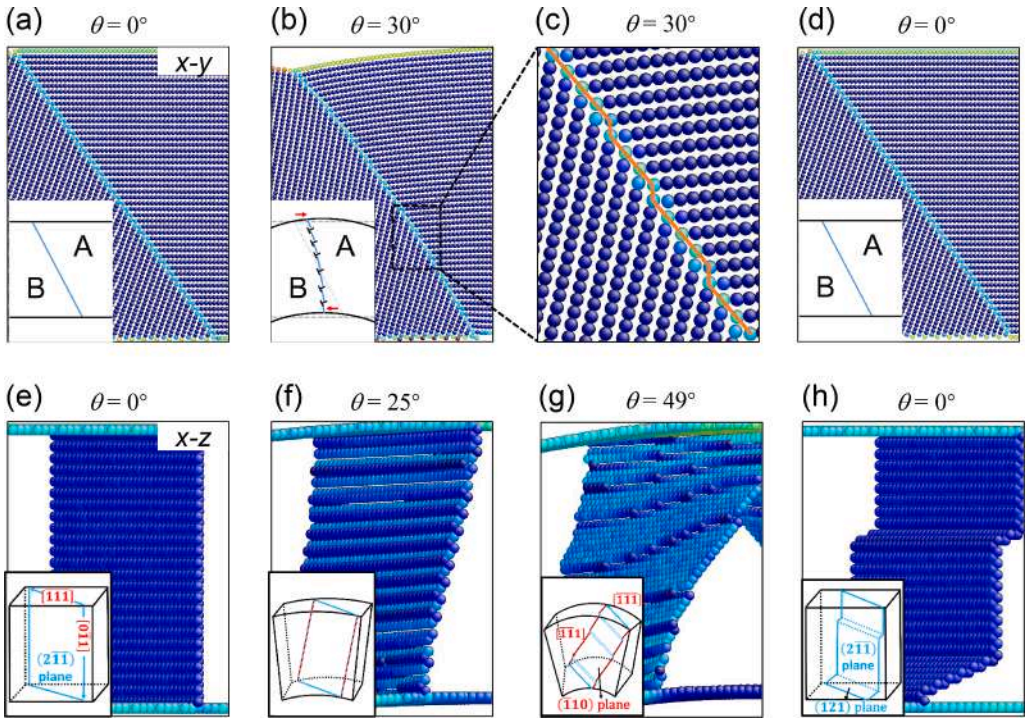

Fig. 5. Illustration of structure change upon loading and unloading for the *xy*-bending and *xz*-bending. (a)-(d) The motion of {112}/⟨111⟩ twin boundary for the *xy*-bending. The curved twin boundary is accommodated by partial dislocations, forming kinks (steps) at the twin boundaries. (e)-(h) The formation of the nonconventional {110} interfaces for the *xz*-bending. The insets in (a), (b), and (d) show the formation of kinks schematically. The insets of (e)-(h) show the transformation from the {112} twin plane to the {110} interfaces.

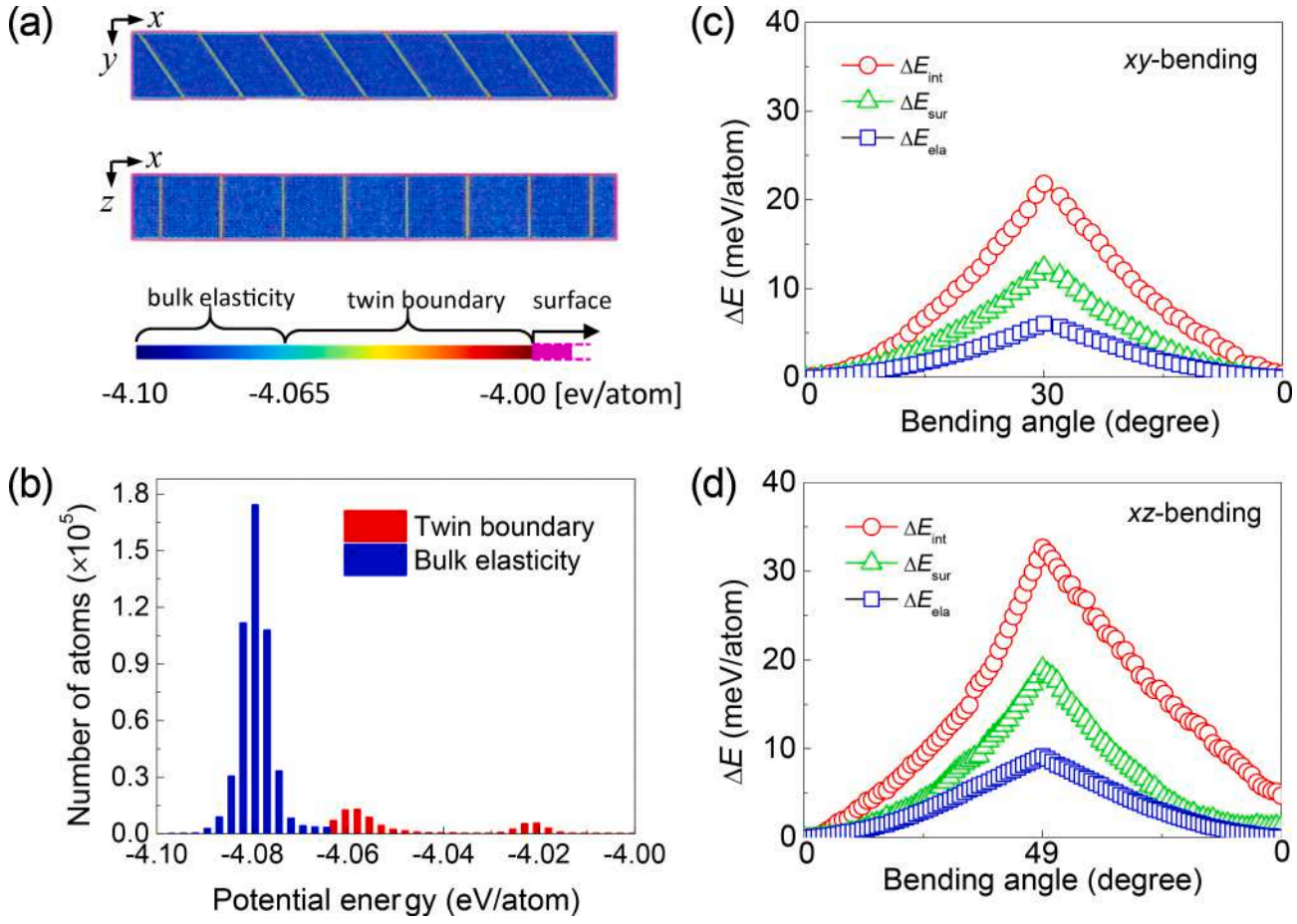

Fig. 6. Energetic analysis of bending deformation under loading and unloading. (a) Distribution of potential energy in the undeformed nanowire ($\theta = 0°$). The colors are coded according to the atomic potential energy. (b) Distribution of atoms according to the potential energy at $\theta = 0°$. (c)-(d) The variation of energy components for the *xy*-bending and *xz*-bending, respectively.

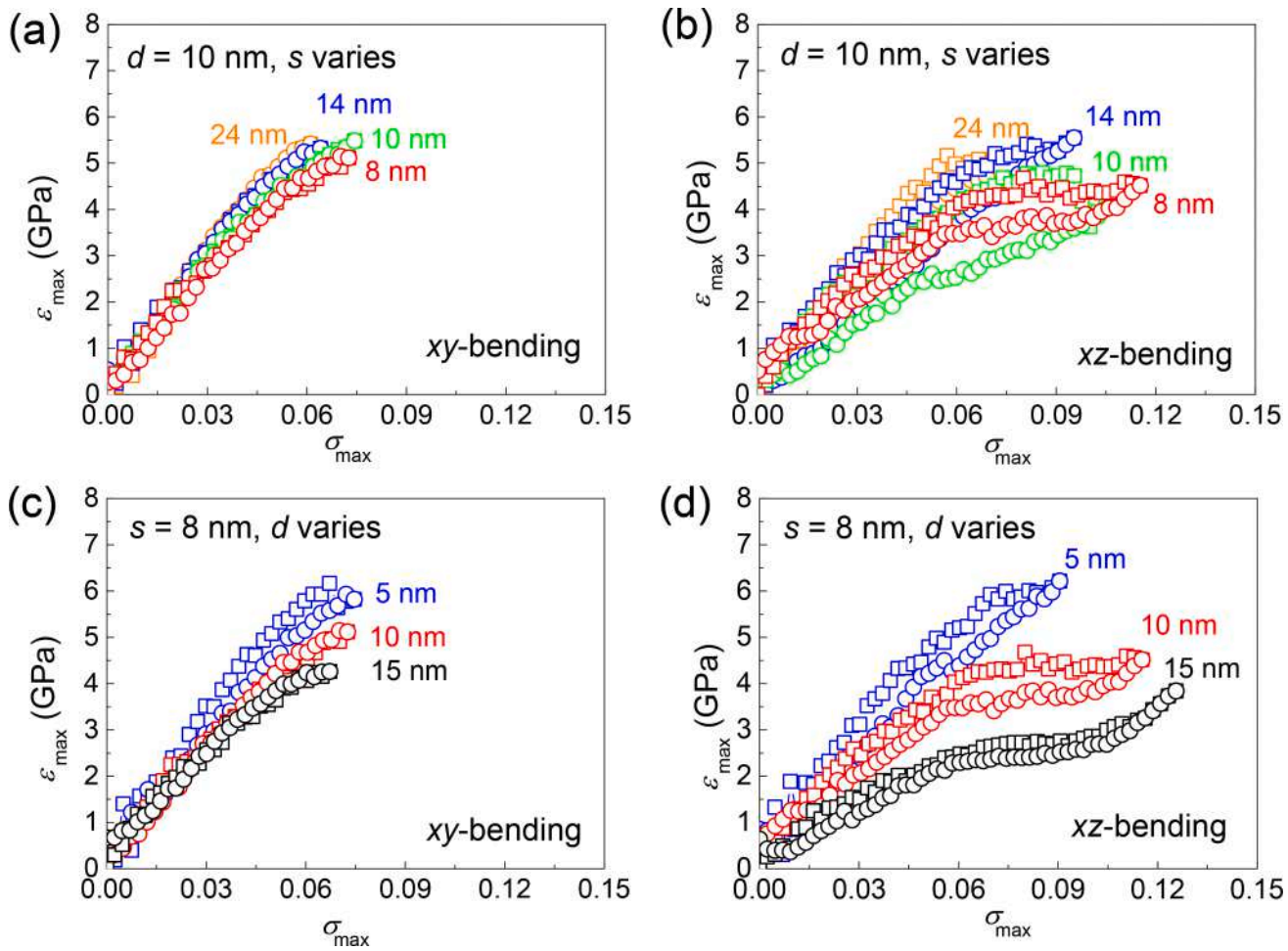

Fig. 7. Size effect on the shape recoverability in the twinned α -Fe nanowires. The variation of σ_{max} as a function of ε_{max} in samples with the fixed d but different s for (a) xy-bending and (b) xz-bending. The variation of σ_{max} as a function of ε_{max} in samples with fixed s but different d for (c) xy-bending and (d) xz-bending.

nonconventional {110} interfaces (Fig. 5e-h). A local ⟨111⟩/{112} "twin" forms in each layer and the "twin plane" of each layer glides via 1/6 ⟨111⟩ partial dislocation upon bending (Fig. 5f). Consequently, various local ⟨111⟩/{112} "twins" form and the whole interface lies in the nonconventional {110} planes. The bent {110} interfaces contain small steps. Further deformation drives the interface growth with smaller {110} interfaces merging into larger ones (Fig. 5g). Such {110} interfaces also exhibit good reversible motion under unloading, even some "defects" left after unloading (Fig. 5h) [6].

3.3. Driving force for the shape recovery

We then carried out the energetic analysis upon bending deformation [6]. The deformation energy of the twinned nanowire can be stored as the surface energy ΔE_{sur}, the interface energy ΔE_{int}, and the elastic energy ΔE_{ela}. We roughly define ΔE_{sur} as the energy change of the surface atoms, ΔE_{int} as the energy change of the interface atoms, and ΔE_{ela} as the energy change of the other atoms in bulk sites. The surface atoms are selected as the outmost three layers, which can take account for almost the whole surface energy. The interface and the bulk can be separated via the potential energy. Fig. 6a shows a snapshot of the atomic configurations for the undeformed state at $\theta = 0°$. The energy distributions of the interface and the bulk are shown in Fig. 6b. Overlap exists between the bulk elastic energy and the interfacial energy. The overlap indicates that there is no clear boundary between the interface and the bulk. An energy threshold is determined between elastic and interfacial energy by the criterion that no isolated atoms in the bulk should contribute to the interface energy. For each component, the energy change is further divided by the corresponding number of atoms in each part to normalize the energy in unit of meV per atom.

Fig. 6c and d show the variation of different energy components upon loading and unloading in xy-bending and xz-bending, respectively. ΔE_{int}, ΔE_{sur} and ΔE_{ela} increase upon loading and decrease upon unloading, indicating that they all contribute to the driving force for the shape recovery in bending pseudoelasticity. The energy change of the interface is the largest (about 24 meV/atom for xy-bending and 33 meV/atom for xz-bending). Such high interface energy arises from the core energy of the stored partials for the xy-bending and the highly deformed {110} interface for the xz-bending. In addition, the nanowires have a high surface-to-volume ratio [26,27], the surface energy difference between the deformed and undeformed states also provide certain driving force for shape recovery.

4. Discussion

4.1. Size-effect of pseudoelasticity

We further carried out a set of simulations to study the size effect of the pseudoelasticity. The twinned nanowires can be characterized by two lengthscale parameters, i.e. wire side width d (external length scale) and twin boundary spacing s (internal length scale). We first fixed d to 10 nm and varied s as 8 nm, 10 nm, 14 nm and 24 nm. The variation of σ_{max} with ε_{max} upon loading and unloading in different samples are shown in Fig. 7a and b. The magnitude of maximum recoverable strain

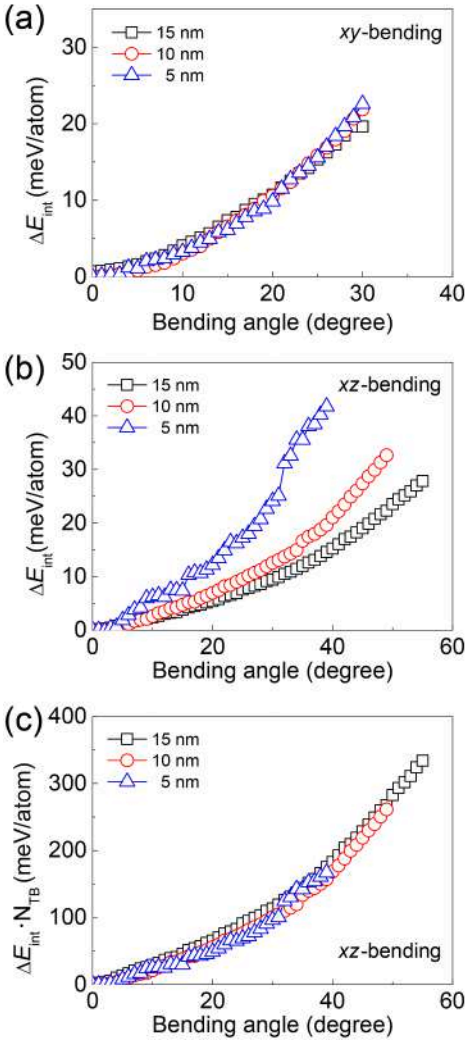

Fig. 8. Variation of ΔE_{int} as a function of bending angle in twinned α -Fe nanowires with a fixed s but different d for (a) xy-bending and (b) xz-bending. (c) The variation of $\Delta E_{int} \cdot N_{TB}$ as a function of bending angle for the xz-bending.

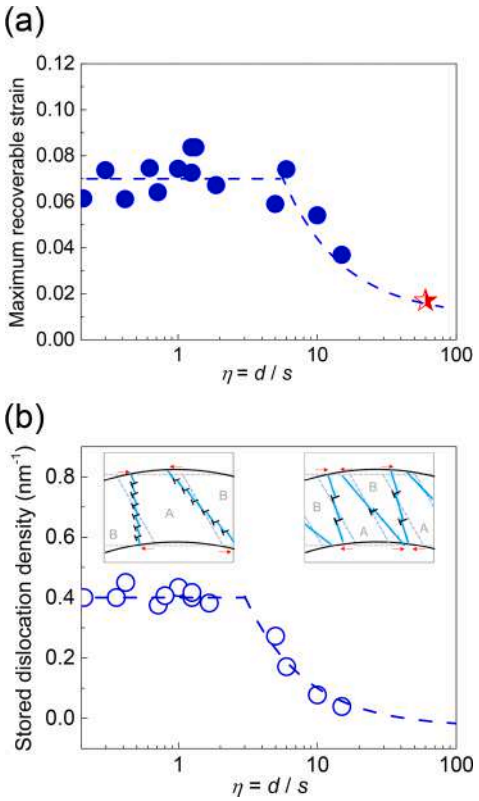

Fig. 9. Size effect on shape recoverability in twinned α -Fe nanowires for the xy-bending. (a) The variation of maximum recoverable strain $\varepsilon_{max}^{recovery}$ and (b) density of stored partial dislocations per TB as a function of η. The dashed lines are guide for eyes. The insets illustrate the accumulation of partial dislocations at the interfaces schematically in the two distinct regimes.

$\varepsilon_{max}^{recovery}$ lies in a narrow range 0.06 ~ 0.08 for the xy-bending (Fig. 7a). However, $\varepsilon_{max}^{recovery}$ decreases with the increase of s for the xz-bending (Fig. 7b).

Then we fixed s to 8 nm and varied d as 5 nm, 10 nm and 15 nm. The bending stress–strain curves are shown in Fig. 7c and d for the xy- and xz-bending. We found a "smaller is stronger" effect. The $\varepsilon_{max}^{recovery}$ remains almost the same for xy-bending (Fig. 7c), leading to the weak size dependence. However, $\varepsilon_{max}^{recovery}$ decreases with decrease of d, resulting in a stronger size effect. To understand the difference of size dependency, we calculated the interface energy upon bending for the samples with a fixed s but different d (5 nm ~ 15 nm). Fig. 8a shows the variation of interface energy ΔE_{int} as a function of bending angle for the xy-bending. The increment of ΔE_{int} is related to the core energy of partial dislocations stored at the TBs. The close ΔE_{int} in different samples indicates a close partial dislocation density stored at each twin plane, which leads to a weak size dependence on shape recovery. However, for the xz-bending, the increment rate of ΔE_{int} decreases with the increase of sample size (Fig. 8b). This indicates that the transformed {110} interfaces undergo larger deformation for smaller samples. We further normalized the increment of interface energy as $\Delta E_{int} \cdot N_{TB}$, where N_{TB} refers to the number of TBs. We found the normalized interface energy is independent on sample size d (Fig. 8c). When the samples undergo the same amount of strain, sample with more TBs undergoes smaller deformation of TBs and therefore exhibits a better shape recoverability.

4.2. Characterization of shape recoverability with the ratio of η

We defined the ratio η of the wire side width d to the twin boundary spacing s. The number of TBs in a sample is proportional to the ratio $\eta = d/s$. We collect the maximum recoverable strain $\varepsilon_{max}^{recovery}$ in different samples with d = 5 nm ~ 15 nm and s = 1 nm ~ 60 nm. The variation of $\varepsilon_{max}^{recovery}$ as a function of η for xy-bending is shown in Fig. 9. Two distinct regimes could be identified (Fig. 9a). The magnitude of $\varepsilon_{max}^{recovery}$ lies in a narrow range 0.06 ~ 0.08 when $\eta < 6$. However, it decreases inversely with the increase of η when $\eta > 6$. Owing to high computational cost, η is limited to 15 in our simulations. We mark the experimental value of $\varepsilon_{max}^{recovery}$ of bulk Cu-Al-Ni [10] as a red star in Fig. 9a. We found our parameter η can be extended to capture this point quite well (η ~ 60).

The dependency of shape recoverability on η in xy-bending is strongly associated with the competition between the stored partial dislocations at the TBs and the dislocation–dislocation interactions. Bending deformation generates a non-uniform stress, i.e. a gradient stress from tension to compression, which induces the two oriented variants in wedged shapes via the TBs motion (Fig. 1c). This wedged domains have been observed experimentally [11]. As we have shown above, the movement of twin boundaries is completed by the glide of successive partial dislocations. Due to the non-uniform stress, the partial dislocations are stored in the curved interfaces with a certain distance. These dislocations have the same type. Consequently, the repulsive forces are generated between dislocations. Thus, there exists an upper

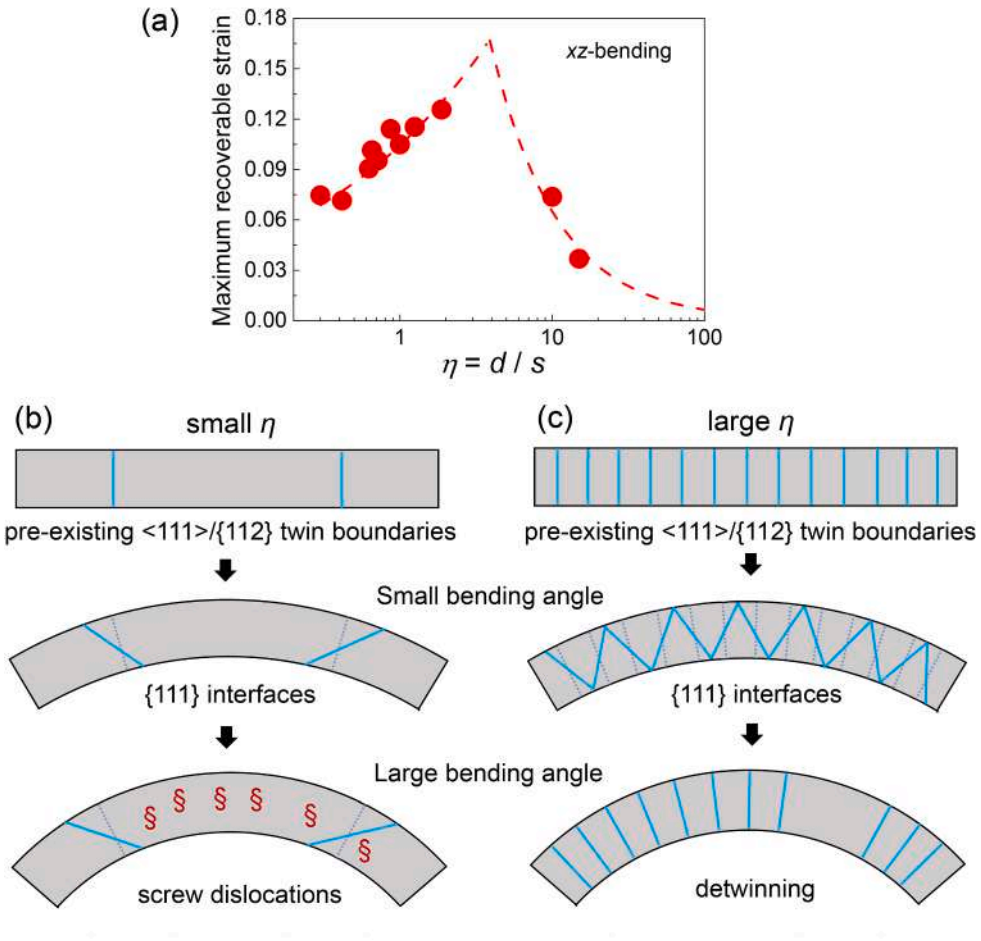

Fig. 10. Size effect on shape recoverability in twinned α -Fe nanowires for the *xz*-bending. (a) The variation of maximum recoverable strain $\varepsilon_{max}^{recovery}$ as a function of η. The dashed lines are guide for eyes. Schematic illustration of deformation mechanism for samples with (b) smaller η and (c) larger η.

bound for the stored dislocation density at the TBs. The real maximum recovery strain depends on the density of partials. For samples with smaller η, each TB deforms more independently due to a relatively large twin spacing. Thus, the interactions between twin boundaries are very weak. We found the stored dislocation density becomes saturated for sample with $\eta < 6$ (Fig. 9b), resulting in an almost constant of $\varepsilon_{max}^{recovery}$. However, samples with a larger η contain denser twin boundaries. When the twin boundaries move closer upon large bending angle, the interactions between the curved TBs become stronger, which could weaken the capability of TBs to store more dislocations and the shape recoverability (Fig. 9b). As η becomes larger, we found that the $\varepsilon_{max}^{recovery}$ almost follows inversely with η.

For the *xz*-bending, the variation of $\varepsilon_{max}^{recovery}$ as a function of η can also be identified as two distinct regions (Fig. 10a). $\varepsilon_{max}^{recovery}$ increases with the increase of η for smaller η, but decreases with the increase of η for larger η. The peak value of $\varepsilon_{max}^{recovery}$ is estimated to occur at $\eta = 5$. The η-dependent shape recoverability is close related to the transformation from the original {112} twin boundaries to the nonconventional {110} interfaces. For a sample with smaller η, there are little TBs sharing deformation strains. Dislocations are easily generated from the interfaces and interact with {110} interfaces, producing the unrecoverable strain (Fig. 10b). Most of these dislocations are 1/2 ⟨111⟩ full screw dislocations. Thus, the sample can sustain a larger recoverable bending deformation with the increase of η. Nevertheless, detwinning could occur for the nanowires with a very high η (Fig. 10c). This would also weaken the reverse transformation of {110} interfaces to the {112} twin boundaries.

4.3. Association with experimental observations

The pseudoelastic behavior of Cu-Al-Ni alloys under bending have been observed experimentally many years ago [10]. The pseudoelasticity occurs below the critical temperature for martensitic transformation, where no phase transformation is induced under mechanical loading. The evolution of domain pattern is proposed to be responsible for the shape recovery. However, there is still lack of atomic/microscopic level understanding on such behavior in the early studies. Here we observed a similar phenomenon in twinned α-Fe nanowires. We found the shape recovery is close related to the movement and bending of twin boundaries using atomistic simulations. We observed that a high density of partial dislocations are stored in the curved twin boundaries upon bending. The curved interfaces have a high interfacial energy and provides the primary driving force for shape recovery.

Recently, twinning induced pseudoelasticity have been observed by transmission electron microscopy (TEM) techniques in bcc tungsten [1]. Moreover, the kinked TBs have been characterized in the bent tungsten [3], which keeps accordance with our atomistic simulations (see Fig. 5b-c). In addition, an unstable twin structure with inclined twin boundary was observed [2]. The Moiré fringes in the TEM images indicate that the twin thickness could be different [2], which might correlate with the formation of non-conventional {110} interface in our simulations. Bending induced pseudoelasticity was also experimentally observed in other materials such as GaP whiskers [28], Si nanowires [29] and $BaTiO_3$ membrane [30] and some metallic whiskers [24,31]. Among these experiments, the triangle shaped twin morphology [10] was

clearly captured, similar to that in our simulations.

In nanomaterials, there are many similar recoverable deformation associated with twinned structure [9,32–34]. Several experimental studies have shown the twinned (penta-twinned and bi-twinned) silver nanowires could exhibit the reversible plasticity [9,32,33]. The leading partials nucleate from free surfaces upon loading. These partials interact with the pre-existing twin boundaries and are hindered by twin boundaries, making leading partials trapped in the sample. These partials could be retraced back from the twin boundaries upon unloading, resulting in the shape recovery. In our simulations, the nucleation and retraction of partial dislocations also account for shape recovery for the *xy*-bending in twinned α-Fe nanowires.

5. Conclusions

(a) We studied the mechanical behavior of twinned α-Fe nanowires under bending. The deformation of pre-existing twin boundaries behaves differently when bending along different orientations. The twin boundaries are heavily curved with a high-density 1/6 ⟨111⟩/{112} partial dislocations under bending when the neutral plane intersects with twin plane along $[0\bar{1}1]$ direction. However, the twin boundaries could transform to the nonconventional {110} interfaces under bending when the neutral plane intersects with twin plane along [111] direction.

(b) Bent nanowires show good pseudoelasticity. We characterized the shape recoverability by a ratio η of the nanowire size (external length scale) to twin boundary spacing (internal length scale). For the bending deformation of curved {112} twin boundaries, η depends on the partial density stored at the twin planes. For samples with smaller η, the maximum recoverable strain lies in a narrow range around $0.06 \sim 0.08$ due to a saturated density of partials at each twin boundary. However, the maximum recoverable strain drops with the increase of η when $\eta > 6$ because the storage capability is weakened by strong interactions between twin boundaries.

(c) For the pseudoelasticity based on the transformation of {110} interfaces, the peak value of maximum recoverable strain occurs around $\eta = 5$. For samples with smaller η, dislocations are easily generated and interact with {110} interfaces, producing the unrecoverable strain. However, detwinning occurs for samples with larger η, which weakens the reversible transformation of {110} interfaces to the {112} twin boundaries.

CRediT authorship contribution statement

Yang Yang: Investigation, Methodology, Software, Writing - original draft. **Suzhi Li:** Investigation, Supervision, Writing - review & editing. **Xiangdong Ding:** Funding acquisition, Supervision, Writing - review & editing. **Jun Sun:** Funding acquisition, Supervision.

Declaration of Competing Interest

The authors declare that they have no known competing financial interests or personal relationships that could have appeared to influence the work reported in this paper.

Acknowledgements

X.D. and J.S. appreciate the support of NSFC (51320105014, 51621063) and 111 project (BP2018008). S.L. appreciates the support from the NKRDPC (Grant No. 2019YFA0307900).

References

[1] J. Wang, Z. Zeng, C.R. Weinberger, Z. Zhang, T. Zhu, S.X. Mao, In situ atomic-scale observation of twinning-dominated deformation in nanoscale body-centred cubic tungsten, Nat. Mater. 14 (6) (2015) 594.
[2] X. Wang, J. Wang, Y. He, C. Wang, L. Zhong, S.X. Mao, Unstable twin in body-centered cubic tungsten nanocrystals, Nat. Commun. 11 (1) (2020) 1–7.
[3] S. Wei, Q. Wang, H. Wei, J. Wang, Bending-induced deformation twinning in body-centered cubic tungsten nanowires, Mater. Res. Lett. 7 (5) (2019) 210–216.
[4] S. Li, X. Ding, J. Deng, T. Lookman, J. Li, X. Ren, J. Sun, A. Saxena, Superelasticity in bcc nanowires by a reversible twinning mechanism, Phys. Rev. B 82 (20) (2010), 205435.
[5] S. Li, X. Ding, J. Li, X. Ren, J. Sun, E. Ma, High-efficiency mechanical energy storage and retrieval using interfaces in nanowires, Nano Lett. 10 (5) (2010) 1774–1779.
[6] Y. Yang, S. Li, X. Ding, J. Sun, E.K.H. Salje, Interface driven pseudo-elasticity in α-Fe nanowires, Adv. Funct. Mater. 26 (5) (2016) 760–767.
[7] S. Li, E.K.H. Salje, S. Jun, X. Ding, Large recovery of six-fold twinned nanowires of α-Fe, Acta Mater. 125 (2017) 296–302.
[8] Y. Yang, S. Li, X. Ding, J. Sun, J. Weiss, E.K.H. Salje, Twisting of pre-twinned α-Fe nanowires: from mild to wild avalanche dynamics, Acta Mater. 195 (2020) 50–58.
[9] Q. Qin, S. Yin, G. Cheng, X. Li, T.-H. Chang, G. Richter, Y. Zhu, H. Gao, Recoverable plasticity in penta-twinned metallic nanowires governed by dislocation nucleation and retraction, Nat. Commun. 6 (1) (2015) 1–8.
[10] K. Otsuka, H. Sakamoto, K. Shimizu, A new type of pseudoelasticity in single variant twinned Martensites, Scripta Metall. 11 (1) (1977) 41–46.
[11] H.D. Chopra, C. Bailly, M. Wuttig, Domain structures in bent In-22.5 at.% Tl polydomain crystals, Acta Mater. 44 (2) (1996) 747–751.
[12] M. Wuttig, L. Chun-Hung, Twinning pseudoelasticity in In-Tl, Acta Metall. 31 (7) (1983) 1117–1122.
[13] E.K.H. Salje, H. Zhang, Domain boundary engineering, Phase Transit. 82 (6) (2009) 452–469.
[14] M.I. Mendelev, S. Han, D.J. Srolovitz, G.J. Ackland, D. Sun, M. Asta, Development of new interatomic potentials appropriate for crystalline and liquid iron, Philos. Mag. 83 (35) (2003) 3977–3994.
[15] M.S. Daw, M.I. Baskes, Embedded-atom method: derivation and application to impurities, surfaces, and other defects in metals, Phys. Rev. B 29 (12) (1984) 6443.
[16] M. Tanaka, E. Tarleton, S.G. Roberts, The brittle–ductile transition in single-crystal iron, Acta Mater. 56 (18) (2008) 5123–5129.
[17] W.G. Hoover, Canonical dynamics: equilibrium phase-space distributions, Phys. Rev. A 31 (3) (1985) 1695.
[18] S. Nosé, A unified formulation of the constant temperature molecular dynamics methods, J. Chem. Phys. 81 (1) (1984) 511–519.
[19] S. Plimpton, Fast parallel algorithms for short-range molecular dynamics, J. Comput. Phys. 117 (1) (1995) 1–19.
[20] J. Li, AtomEye: an efficient atomistic configuration viewer, Modell. Simul. Mater. Sci. Eng. 11 (2) (2003) 173.
[21] A. Stukowski, Visualization and analysis of atomistic simulation data with OVITO–the open visualization tool, Modell. Simul. Mater. Sci. Eng. 18 (1) (2009), 015012.
[22] A. Stukowski, K. Albe, Dislocation detection algorithm for atomistic simulations, Modell. Simul. Mater. Sci. Eng. 18 (2) (2010), 025016.
[23] A.M. Howatson, P.G. Lund, J.D. Todd, Engineering Tables and Data, Chapman and Hall, London, 1972.
[24] G.W. Sears, A. Gatti, R.L. Fullman, Elastic properties of iron whiskers, Acta Metall. 2 (5) (1954) 727–728.
[25] C.L. Kelchner, S.J. Plimpton, J.C. Hamilton, Dislocation nucleation and defect structure during surface indentation, Phys. Rev. B 58 (17) (1998) 11085.
[26] J. Diao, K. Gall, M.L. Dunn, Surface-stress-induced phase transformation in metal nanowires, Nat. Mater. 2 (10) (2003) 656.
[27] S. Li, X. Ding, J. Li, X. Ren, J. Sun, E. Ma, T. Lookman, Inverse martensitic transformation in Zr nanowires, Phys. Rev. B 81 (24) (2010), 245433.
[28] E. Schönherr, E. Winckler, Bending and straightening of GaP whiskers during their growth, J. Cryst. Growth 32 (1) (1976) 117–122.
[29] G. Stan, S. Krylyuk, A.V. Davydov, I. Levin, R.F. Cook, Ultimate bending strength of Si nanowires, Nano Lett. 12 (5) (2012) 2599–2604.
[30] G. Dong, S. Li, M. Yao, Z. Zhou, Y.-Q. Zhang, X. Han, Z. Luo, J. Yao, B. Peng, Z. Hu, Super-elastic ferroelectric single-crystal membrane with continuous electric dipole rotation, Science 366 (6464) (2019) 475–479.
[31] S.S. Brenner, C.R. Morelock, The high-temperature recovery of deformed copper whiskers, Acta Metall. 4 (1) (1956) 89–90.
[32] R.A. Bernal, A. Aghaei, S. Lee, S. Ryu, K. Sohn, J. Huang, W. Cai, H. Espinosa, Intrinsic Bauschinger effect and recoverable plasticity in pentatwinned silver nanowires tested in tension, Nano Lett. 15 (1) (2015) 139–146.
[33] G. Cheng, S. Yin, C. Li, T.-H. Chang, G. Richter, H. Gao, Y. Zhu, In-situ TEM study of dislocation interaction with twin boundary and retraction in twinned metallic nanowires, Acta Mater. 196 (2020) 304–312.
[34] H.S. Park, K. Gall, J.A. Zimmerman, Shape memory and pseudoelasticity in metal nanowires, Phys. Rev. Lett. 95 (25) (2005), 255504.